Langmuir

Article

pubs.acs.org/Langmuir

Lipid–Lipid Interactions in Aminated Reduced Graphene Oxide Interface for Biosensing Application

Md. Azahar Ali,[†,‡,$] K. Kamil Reza,[†,$] Saurabh Srivastava,[†] Ved Varun Agrawal,*[,†] Renu John,*[,‡] and Bansi Dhar Malhotra*[,†,§]

[†]Department of Science and Technology Centre on Biomolecular Electronics, Biomedical Instrumentation Section, CSIR-National Physical Laboratory, Dr. K. S. Krishnan Marg, New Delhi, Delhi 110012, India

[‡]Indian Institute of Technology Hyderabad, Ordnance Factory Estate, Yeddumailaram, Hyderabad, Andhra Pradesh 502205, India

[§]Department of Biotechnology, Delhi Technological University, Shahbad Daulatpur, Main Bawana Road, Delhi, Delhi 110042, India

Supporting Information

ABSTRACT: A label-free biosensor based on antiapolipoprotein B 100 functionalized-aminated reduced graphene oxide interface has been fabricated for detection of low density lipoprotein (LDL or lipid) cholesterol. The aminated reduced graphene oxide (NH_2-rGO) based electrode surface is covalently functionalized with antiapolipoprotein B 100 (AAB or lipid) using EDC/NHS coupling chemistry. The lipid–lipid interactions at the NH_2-rGO electrode surface have been investigated using electrochemical impedance spectroscopic technique. The structural and morphological investigations of NH_2-rGO based immunosensor have been accomplished via transmission electron microscopy, X-ray diffraction, Fourier transform infrared spectroscopy, UV–visible, and electrochemical techniques. The impedimetric response of the proposed immunosensor shows excellent sensitivity (612 Ω mg^{-1} dL cm^{-2}), a response time of 250 s, and a low detection limit of 5 mg/dL of LDL molecules. The association, dissociation, and equilibrium rate constants for this immunoelectrode are found to be 1.66 M^{-1} s^{-1}, 0.6 s^{-1}, and 2.77 M^{-1}, respectively. The long-term stability and excellent reproducibility of the proposed immunosensor indicates a suitable platform for detection of LDL or lipid molecules. This immunosensor provides an efficient platform for analysis of the antigen–antibody interactions of lipid molecules.

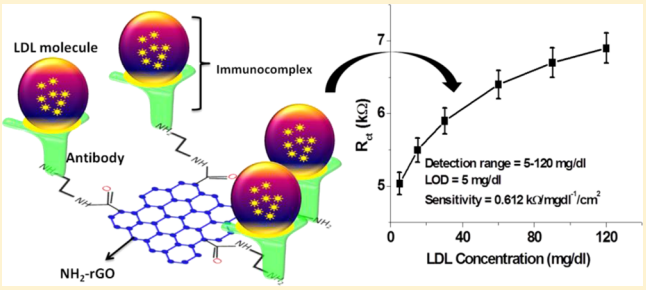

1. INTRODUCTION

There is increased interest toward the development of point-of-care (POC) diagnostic devices for the detection of clinically important biomolecules such as tyrosine, micro-RNA or DNA, glucose, and cholesterol.[1−3] With recent developments in the emerging field of nanotechnology and nanofabrication, metallic and metal oxide nanostructures[4−6] have been considered as interesting electrochemical-based biosensor platforms with many advantages compared to those of the existing biosensing devices. Carbon allotropes like graphene oxide, carbon nanotubes, nanofibers, and fullerenes are being explored for development of electrochemical biosensing platforms. The various properties of graphene oxide (GO) such as electrochemical conductivity, stability, and superior mechanical flexibility combined with its finite dimension and unique structure make it a promising candidate for the fabrication of biosensors for detection of the desired biomolecule.[7−9] GO is a chemically modified form of graphene that is known to be an electrical insulator. The availability of functional groups on the basal plane as well as on the edges of GO facilitates heterogeneous electron transport (HET) in an electrochemical biosensor.[10] However, the functional groups such as carboxyl, hydroxyl, epoxy, etc. present in the GO sheets provide limited applications for electrochemical devices due to its high electrical resistance. The chemical reduction of these functional groups results in reduced graphene oxide (rGO) that exhibits enhanced electrical conductivity. Moreover, rGO enriched with hydrophilic functional groups could be used for functionalization of given biomolecules.[10−12] Apart from detection of biomolecules, rGO has been predicted to have applications in bioimaging, drug delivery, and photothermal therapy.[13]

The electro-active sites of rGO, due to the presence of abundant oxygen containing groups (carboxyl groups) attached to its honeycomb like six-atom carbon rings, may promote fast HET rates.[14,15] It has been found that edge-plane of the rGO exhibits a HET rate (k_e) of the order of ∼0.01 cm/s, the basal plane is effectively inert, with k_b (basel plane) lower than 10^{-9} cm/s. The high density of the edge-plane-like defective sites on rGO provides many active sites and may be utilized for

Received: December 31, 2013
Revised: March 10, 2014
Published: March 27, 2014

accelerated electron transfer between the electrode and bulk solution.[16] Moreover, it has been reported that sheet resistance of rGO-based film is higher (1 k to 70 k Ω/sq, <80% transmittance) compared to that of the indium tin oxide (ITO). This characteristic may play an important role in the development of rGO-based impedimetric biosensor. In addition, rGO exhibits high affinity toward H_2O_2 due to superior electrocatalytic activity.[12] This is because of the high density of edge-plane-like defective sites on rGO that provides many active sites for HET.[17] Such significant lowering of the overpotential of the rGO-based electrode for H_2O_2 reduction may perhaps lead to high selectivity. The aminated rGO may also facilitate higher loading of biomolecules due to the covalent bond formation with specific F_c site of the antibody for the development of immunosensor.[18,19]

Eda et al. have demonstrated reduction of the GO for uniform and controllable deposition of 1−5 nm rGO thin films at room temperature on a variety of substrates with desired sheet resistance.[20] Jung et al. have developed a fluorescence resonance energy transfer-based immunosensor using aminated rGO and gold nanoparticles for pathogen detection. Aminated rGO can be functionalized with biomolecules resulting in improved chemical stability.[21] A graphene-based glucose biosensor using covalent binding has been recently reported.[19] The antiaflatoxin functionalized rGO has been utilized for the development of a sensitive food toxin electrochemical biosensor.[22]

Impedimetric spectroscopy is an interesting label-free technique that may yield rapid, simple, and low-cost detection.[16] It can be used to provide detailed information on biorecognition events (such as antigen−antibody, lipid−lipid, lipid−protein interactions, etc.) induced by capacitance and resistance changes on electrode and electrolyte interface.[23] It can be utilized to measure the complex electrical impedance of the electrochemical system arising as a result of electrochemical reaction at the electrode surface due to charge transfer among the reactants. The impedance spectrum can be analyzed by an equivalent circuit consisting of resistances and capacitances resulting due to physicochemical process like diffusion system.[24,25] The impedance can be determined by applying a small voltage to the system and simultaneously measuring the current response in terms of Nyquist plot (combination of real and imaginary part of impedance) at different frequencies.[21]

Cholesterol is a janus-faced molecule. It is useful in cell membranes and controls the membrane permeability and fluidity. In a blood stream, low density lipoprotein (LDL; dia: 18−24 nm) or lipid molecules with a density range between 1.019 and 1.063 kg/L carry 60−70% of the serum cholesterol. Interaction of antiapolipoprotein B 100 with sulfated glycosaminoglycans may result in cholesterol accumulation in the arterial walls that in turn perhaps leads to plaque formation resulting in the narrowing of the arteries making these less flexible causing various heart and vascular diseases.[26] Matharu et al. have reported an LDL immunosensor via specific LDL-heparin interaction using a surface plasmon resonance (SPR) technique.[27] Jie et al. have fabricated a cadmium sulfide nanocrystal based immunosensor for LDL detection using electroluminescence phenomenon.[28] Thus, the strategy based on the formation of an immunocomplex (via antigen−antibody interaction) for LDL detection may perhaps provide an efficient platform compared to those based on techniques like nuclear magnetic resonance spectroscopy, Friedewald equation, ultra-centrifugation, electrophoresis, etc.

In this paper, we propose a NH_2-rGO based electrochemical transducer for detection of low density lipoprotein molecules via electrochemical impedimetric spectroscopy (EIS) technique. Besides this, efforts have been made to delineate the interactions and reaction kinetics between lipid (LDL) molecules and antilipid (AAB or antiapolipoprotein B) molecules on rGO interface. The electron microscopic and elemental studies have been conducted to attest the morphology and confirm the functionalization of amine groups with the LDL biomolecule in the rGO matrix.

2. MATERIALS AND METHODS

Chemicals. Graphite powder flakes (45 μm, >99.99 wt%) are procured from Sigma Aldrich, USA. Low density lipoproteins from human plasma (LDL; MW: 3500 kDa), antiapolipoprotein B-100 (AAB; MW: 515 kDa), bovine serum albumin (BSA), N-hydroxysuccinimide (NHS), N-ethyl-N0-(3-dimethylaminopropyl carbodiimide) (EDC), thyonyl chloride ($SOCl_2$), tetrahydrofuran (THF), and ethelenediamine (EDA) are purchased from Sigma−Aldrich (USA). Distilled water is from the Millipore water purification system. Lyophilized powder (5 mg) of LDL is reconstituted with 1 mL of deionized water to make a solution containing 150 mM NaCl of pH 7.4 and 0.01% ethylenediaminetetraacetic acid (EDTA). Solution of BSA (2 mg/mL) is prepared in 50 mM phosphate buffer saline (PBS) pH 7.4 containing 150 mM NaCl. The AAB solution (1 mg/mL) is prepared in 50 mM phosphate buffer saline (PBS) solution pH 7.4 containing 150 mM NaCl.

Synthesis of NH_2-Reduced Graphene Oxide. The GO powder has been synthesized using the modified Hummer's method and is reduced using a prcocedure according to an earlier report.[22] The rGO (0.1 mg) is sonicated in 50 mL of $SOCl_2$ solution for 30 min at room temperature (25 °C). This suspension is refluxed under magnetic stirring for 48 h and then filtered. The filtered powder is washed with THF and is kept for drying under vacuum conditions for about 20 min. The rGO powder is added to excessive EDA $[NH_2(CH_2)_2\ NH_2]$ via magnetic stirring at room temperature for 10 h. This mixture is used for washing with THF and then filtered. This filtered powder is dried at 80 °C for 10 h. This process leads to the replacement of thionyl chloride (COCl) with the amide group (CO-NH) on the edges of rGO sheet. Among the two NH_2 groups, one is used for amide bond formation with the COOH group of rGO via CO-NH, while the other group is free on the rGO sheet.[29] This solution is stable for a period of two weeks, without any sign of aggregation. The chemically active NH_2-rGO is obtained containing a considerable amount of functional ($-NH_2$) groups for covalent attachment of antibodies via amide bond formation.

Fabrication of the NH_2-rGO/ITO Electrode. Chemically synthesized NH_2-rGO is deposited on ITO coated glass substrate via the electrophoretic deposition (EPD) technique.[30,31] First, a well-dispersed stock solution of NH_2-rGO (50 mg dL^{-1}) in acetonitrile is prepared via ultrasonication (40 W, 0.25 A) for about 4 h. 500 μL of this stock solution is dispersed in 10 mL of acetonitrile to obtain a dilute colloidal suspension of NH_2-rGO that has been used for deposition. The electrophoretic deposition is carried out using a two electrodes cell containing the colloidal suspension by applying DC voltage (65 V) for about 5 min. In order to get surface charges on the NH_2-rGO, 10^{-5}−10^{-4} mol of $Mg(NO_3)_2{\cdot}6H_2O$ is added into the suspension as an electrolyte for EPD. A platinum foil (1 cm × 2 cm) acts as the cathode and a precleaned ITO-coated glass substrate (size; 0.5 cm^2, sheet resistance; 30 Ω cm^{-1}) as the anode. The two electrodes are placed parallel to each other separated by 1 cm and dipped in the NH_2-rGO colloidal suspension. The deposited film is then removed from the suspension and washed with deionized water followed by drying at 100 °C.

Fabrication of Immunosensor. Twenty μL of AAB solution is uniformly spread on the NH_2-rGO/ITO electrode surface and kept in a humid chamber for about 6 h and then stored at 4 °C. The covalent interaction occurs between the free $-NH_2$ groups of rGO and the

dx.doi.org/10.1021/la4049852 | Langmuir 2014, 30, 4192−4201

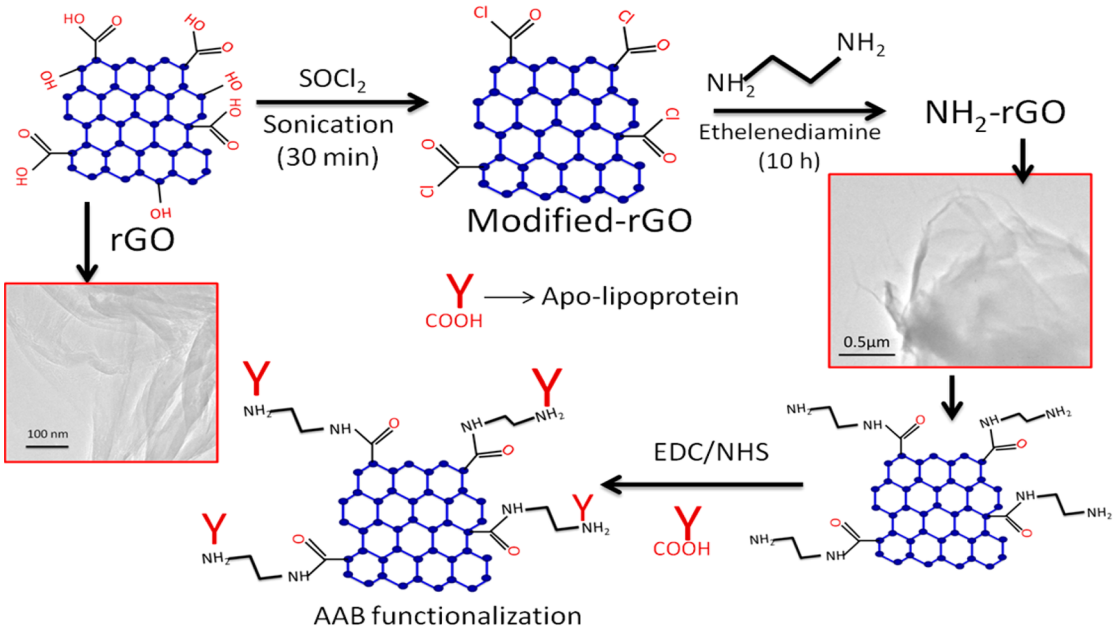

Figure 1. Apo-lipoprotein B 100 functionalization on an NH_2-rGO sheet for LDL detection.

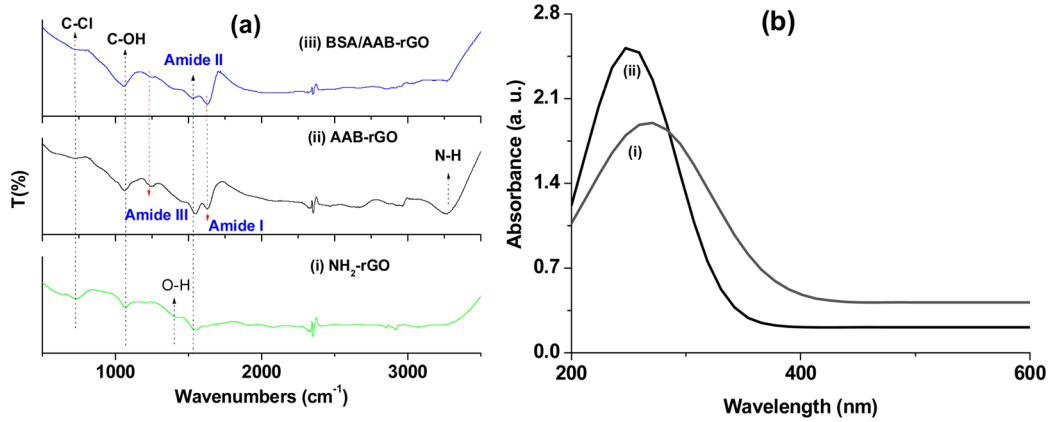

Figure 2. (a). FT-IR studies of various NH_2-rGO films and (b) UV−visible studies of (i) rGO and (ii) AAB-rGO.

−COOH (F_c binding site) groups of AAB using EDC/NHS coupling chemistry. Prior to AAB treatment, the NH_2-rGO/ITO surface is treated with EDC-NHS chemistry in which EDC (0.2 M) works as the coupling agent and NHS (0.05 M) works as an activator. EDC-NHS activates the −COOH group present at the F_c site of AAB antibodies. This results in the formation of a strong amide bond (C-N) between -NH_2 group of NH_2-rGO/ITO and −COOH groups of AAB (Figure 1). The graphene sheets that are not converted to amine terminated; their carboxylic acid groups are perhaps utilized to bind with NH_2 groups of antibody on the transducer surface. The AAB-rGO surface is treated with BSA molecules for blocking the nonspecific active sites of the electrode. The BSA/AAB-rGO/ITO immunoelectrode is then washed with PB and stored at 4 °C, when not in use.

3. RESULTS AND DISCUSSION

3.1. Structural Studies. FT-IR studies have been carried out to investigate the functional groups of the fabricated immunosensor. Figure 2(a) shows FT-IR spectra of the (i) NH_2-rGO/ITO, (ii) AAB-rGO/ITO, and (iii) BSA/AAB-rGO/ITO films. The NH_2-rGO exhibits (spectra i) a characteristic peak at 1414 cm^{-1} corresponding to O−H bending vibration of the carboxyl group. The band seen around 1062 cm^{-1} is due to the C-OH stretching vibration. The band found at 714 cm^{-1} is due to C-Cl stretching in the fingerprint region resulting from $SOCl_2$ modified rGO. A dominant band observed at 1533 cm^{-1} indicates the presence of amide II (60% N-H bending, 40% C-N stretching) due to ethelenediamine treatment of the rGO sheet. After covalent interaction with AAB (spectra ii), additional bands seen at 1248 cm^{-1}, 1628 cm^{-1}, and 3263 cm^{-1} are attributed to amide III (30% C-N stretching + 30% N-H bending + 10% C═O stretching + 10% O═C-N bending + 20% others), amide I (80% C═O stretching + 10% C-N stretching + 10% N-H bending) and N-H stretching, respectively. The intensity of the 1628 cm^{-1} peak is found to be more than that of the NH_2-rGO film due to antibody loading. These results reveal antibody functionalization on the NH_2-rGO surface. The spectra (iii) obtained for the BSA/AAB-rGO/ITO film indicates that there are no changes in the position of the various peaks. However, the intensity of amide I is found to be slightly higher. The UV−vis spectroscopy studies of NH_2-rGO/ITO (a) and AAB-rGO/ITO (b) have been carried out in the wavelength range of 200−800 nm, having the UV source slit width of 2 nm [Figure 2]. It can be seen that the absorption intensity pertaining to the π-π^* transition of aromatic C-C bonds of NH_2-rGO increases monotonically

dx.doi.org/10.1021/la4049852 | Langmuir 2014, 30, 4192−4201

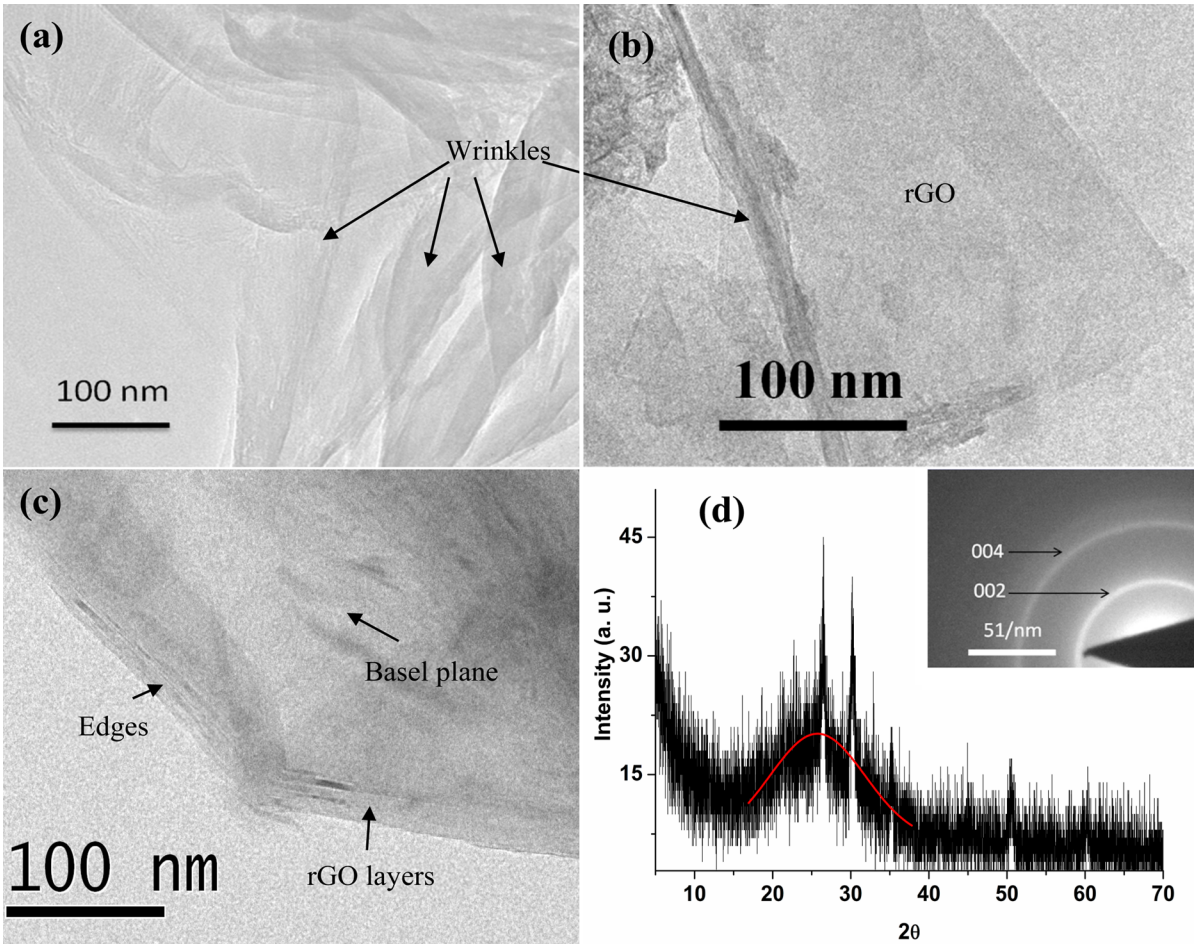

Figure 3. TEM image of rGO before (a) and after (b) NH_2 functionalization. (c) TEM image of NH_2-rGO shows the edges and layers, and (d) X-ray diffraction studies of NH_2-rGO (inset: SAED pattern of NH_2-rGO).

from 390 nm and becomes maximum at 266 nm (curve a). After AAB functionalization on the NH_2-rGO (curve b) surface, the absorption peak is observed to be blue-shifted to 248 nm indicating biofunctionalization of AAB at the rGO electrode surface.

3.2. Microscopic Studies. Figure 3 depicts transmission electron microscopy (TEM) images of rGO before and after NH_2 functionalization. The well-suspended rGO has been prepared in water and is drop cast onto a carbon coated copper grid for the TEM micrograph. Image (a) shows morphology of the rGO prior to NH_2 functionalization. The rGO sheets are overlapped with each other and appear as wrinkles. Image (b) shows TEM image of the rGO after attaching the functional groups of -NH_2. A series of long stranded rGO sheets are clearly visible, that may perhaps be due to incorporation of -NH_2 groups. The image clearly shows the presence of rGO sheets and some of the sheets appear to be crumpled, overlapped, and folded. These overlapped graphene layers result in larger graphene sheets due to aggregation. It can be seen that the overlapped rGO sheets form multilayered graphene and the edges are clearly visible as shown in image (c). The selected area electron diffraction (SAED) pattern indicates crystalline structure of NH_2-rGO [inset (d)]. Two concentric rings of NH_2-rGO appear due to (002) and (004) reflection planes of the graphitic rGO. The X-ray diffraction (XRD) pattern of NH_2-rGO is shown in Figure 3(d). A broad peak appears at 24° (3.7 A°) corresponding to (002) reflection plane indicating formation of rGO. The crystallite size of the synthesized rGO has been determined using the Debye–Scherrer eq 1

$$d = 0.89\lambda/\beta_{002}\cos\theta_{002} \quad (1)$$

where β_{002} is the full width at half-maximum, d_{002} is the interlayer spacing, λ is the wavelength, and θ_{002} is the Bragg angle. The crystallite size of NH_2-rGO has been calculated to be as 0.71 nm. It has been found that the crystallite size of NH_2-rGO is higher than that of the pristine graphite (0.34 nm) due to the introduction of oxygen and nitrogen functional groups in the graphene sheets. These results are in agreement with those of the TEM studies.[22]

We have carried out the quantitative energy-dispersive X-ray spectroscopy (EDX) analysis for elemental confirmation of the synthesized materials such as rGO (i), NH_2-rGO (ii), and BSA/AAB-rGO (iii) [Figure 4]. The results of elemental analysis of these electrodes reveal the traces of nitrogen (N), carbon (C), oxygen (O), and other elements present in rGO, NH_2-rGO, and AAB /NH_2-rGO film, respectively. Table I shows the weight and atomic percentages of various elements obtained for different films. It has been observed that the available weight percentage of C as 76.3% and O as 23.7%, respectively. However, there is no trace of nitrogen element in the rGO film indicating carboxylic functionalization. After amine functionalization, the weight percentage of N element has been found to be around 9 wt% in the NH_2-rGO film resulting in partial

dx.doi.org/10.1021/la4049852 | Langmuir 2014, 30, 4192–4201

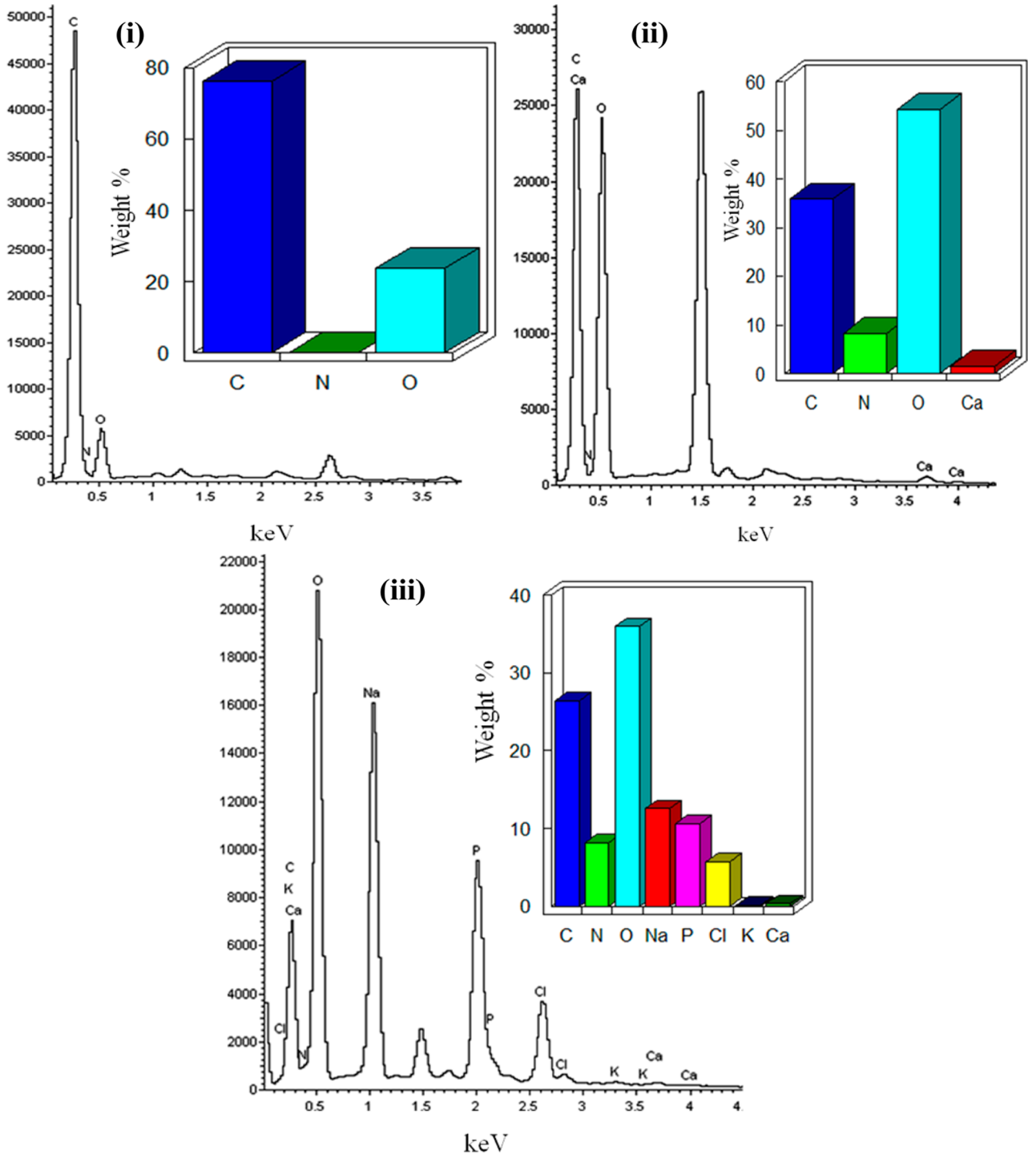

Figure 4. EDX spectra of (i) the rGO/ITO film, inset: quantative composition, (ii) EDX spectra of (i) the NH_2-rGO/ITO film, inset: quantative composition and the BSA/AAB-rGO/ITO film, inset: quantative composition.

amine functionalization of rGO. Further, in the AAB/NH_2-rGO film, we have observed the presence of phosphor (P), sodium (Na), chlorine (Cl), etc. resulting due to attachment of BSA and AAB molecules at the NH_2-rGO surface. These results clearly confirm the functionalization of biomolecules and amine groups at the rGO surface.

3.3. Cyclic Voltammetry (CV) Studies. CV has been used to investigate the electrochemical characteristics of the modified electrode surface. The changes in the peak current and separation of peak potentials in the CV can be related to the electron transfer rate constant i.e. the electron transfer resistance. The CV studies have been conducted for (a) NH_2-rGO/ITO, (b) AAB-rGO/ITO, and (c) BSA/AAB-rGO/ITO electrodes in the PBS containing 5 mM $[Fe(CN)_6]^{3-/4-}$ at 20 mV/s scan rate [Figure 5(i)]. The peak potential separation (ΔE) and peak current (i_a) of the NH_2-rGO/ITO electrode are found to be as 0.26 V and 122 μA, respectively. The ratio of peak current, i_a/i_c, is calculated to be as 1.03 for the NH_2-rGO/ITO electrode indicating a reversible process of the redox species. The peak potential separation (ΔE) of the AAB-rGO/

dx.doi.org/10.1021/la4049852 | *Langmuir* 2014, 30, 4192−4201

Table I. Atomic Concentration (%) of Carbon, Nitrogen, Oxygen, Etc. Presence in rGO, NH_2-rGO, and BSA/AAB-NH_2-rGO

	rGO/ITO		NH_2-rGO/ITO		BSA/AAB-rGO/ITO	
element	weight %	atomic %	weight %	atomic %	weight %	atomic %
C	76.3	81.09	35.83	42.56	26.43	36.10
N	0.0	0.00	8.26	8.41	8.18	9.58
O	23.70	18.91	54.35	48.47	35.96	36.87
Na	--	--	--	--	12.57	8.97
P	--	--	--	--	10.59	5.61
Cl	--	--	--	--	5.76	2.66
Ca	--	--	1.57	0.56	0.34	0.14

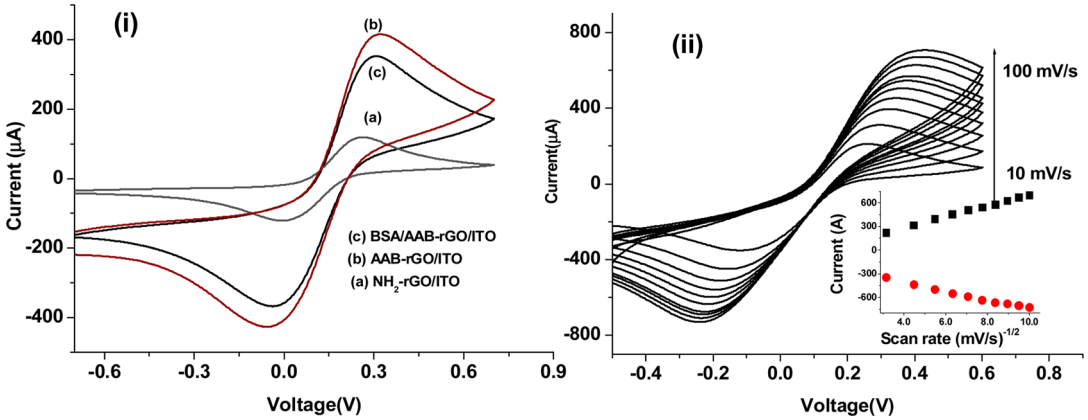

Figure 5. (i) Cyclic voltammetry (CV) of (a) NH_2-rGO/ITO, (b) AAB-rGO/ITO, and (c) BSA/AAB-rGO/ITO electrodes in the PBS containing 5 mM$[Fe(CN)_6]^{3-/4-}$. (ii) CV's of the BSA/AAB-rGO/ITO immunoelectrode as a function of the scan rate (10−100 mV/s).

ITO immunoelectrode is observed to be higher (0.35 V) as compared to that of the NH_2-rGO/ITO electrode. This reveals that the antibody immobilization on the rGO surface causes slower electron transfer toward the electrode in the bulk solution. However, the peak current of the redox species is maximum (416.66 μA) for the AAB-rGO/ITO immunoelectrode compared to that of other electrodes. This is attributed to the larger active surface area in the rGO for immobilization of the enzymes. The anodic peak current of the BSA/AAB-rGO/ITO immunoelectrode is found to be lower (370.84 μA) due to the BSA coating which may block the the diffusion of redox species toward the electrode.[32]

Figure 5(ii) shows CVs of the BSA/AAB-rGO/ITO immunoelectrode obtained as a function of scan rate (10−100 mV/s). The redox peak current increases linearly with the square root of scan rate (inset). The redox peak potential is found to be shifted (i.e., anodic peak potential toward positive and cathodic peak potential toward negative) as the scan rate increases indicating a diffusion control process. The slopes and intercepts can be estimated using eqs 2 and 3

$$i_a = 9.6\,\mu\text{A} + 6.9 \times 10^{-5}\,(\text{A}^2\,\text{mV}^{-1}\,\text{s})^{1/2} \times [\text{scan rate}\,(\text{mV}\,\text{s}^{-1})]^{1/2}; \quad r^2 = 0.998 \tag{2}$$

$$i_c = -191.0\,\mu\text{A} - 5.5 \times 10^{-5}\,(\text{A}^2\,\text{mV}^{-1}\,\text{s})^{1/2} \times [\text{scan rate}\,(\text{mV}\,\text{s}^{-1})]^{1/2}; \quad r^2 = 0.995 \tag{3}$$

The magnitude of charge associated with adsorption or desorption of the adsorbate ions gives an indication of the number of surface catalytic atoms present in the matrix. The electrical charge (Q) is defined as the integral of cell current (I) with respect to time (t)[33] and is given by

$$Q = \int I\,dt \tag{4}$$

The magnitude of charge for the adsorbate ion at the electrode surface (Q_m) and the charge associated with monolayer coverage of the said adsorbate (Q_{ad}) can be related to the electrochemical surface area[33] A_{ec} (cm^2) using eq 5

$$A_{ec} = \frac{Q_{ad}}{Q_m} \tag{5}$$

The effective area obtained for the immunoelectrode (BSA/AAB-rGO/ITO) is estimated to be as 0.23 cm^2 which is higher than that of the AAB-rGO/ITO electrode (0.2 cm^2). This is perhaps due to the coating of BSA at the AAB electrode surface that perhaps results in the conformational change of AAB and provides additional effective electrochemical surface for sensing. The surface charge density[34] (Q_{ads}) of BSA-antibodies adsorption onto the NH_2-rGO/ITO electrode is estimated to be as 4.4×10^{-3} C using the difference between the anodic oxidation and cathodic reduction changes in the presence of the adsorbing protein, after subtracting the small difference between these two charges in the absence of protein via eq 6

$$Q_{ads} = [Q_o^p - Q_r^p] - [Q_o - Q_r] \tag{6}$$

where Q_o^p and Q_r^p, are the surface charge density of anodic and cathodic peak of BSA/AAB-rGO/ITO immunoelectrode, respectively, while Q_o and Q_r are the surface charge density of anodic and cathodic peak of NH_2-rGO/ITO electrode, respectively. The surface concentration of proteins adsorbed on the NH_2-rGO/ITO electrode surface is calculated to be as 1.36×10^{-7} mol/cm^2 using $Q_{ads}M_r/nF$ where n is the number of electrons transferred (1), F is the Faraday constant (96,584 C/mol), and M_r is the molar mass of the BSA and AAB. The

dx.doi.org/10.1021/la4049852 | Langmuir 2014, 30, 4192−4201

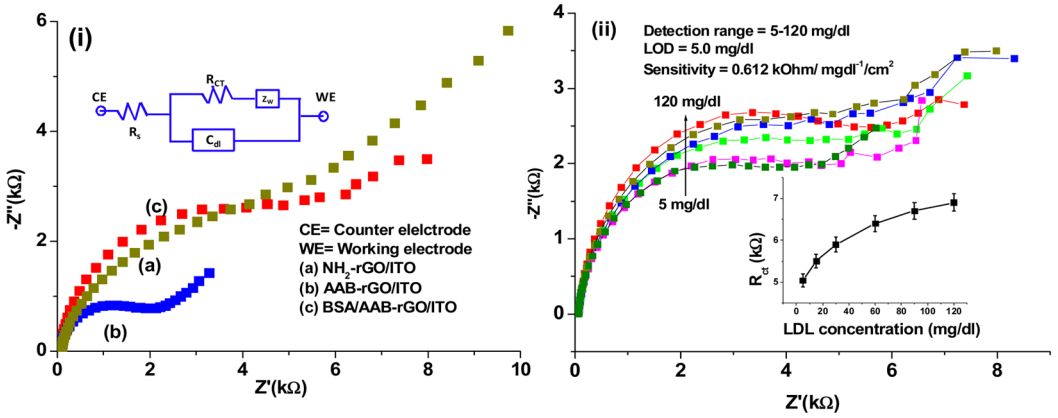

Figure 6. (i) Electrochemical impedance spectra (EIS) of (a) NH_2-rGO/ITO, (b) AAB-rGO/ITO, and (c) BSA/AAB-rGO/ITO electrodes, as a function of frequency ($1-10^4$ Hz) at fix biasing potential 0.01 V (inset: Randles equivalent circuit, where R_S: solution resistance, R_{CT}: charge transfer resistance, Z_W: Warburg impedance, and C_{dl}: double layer capacitance. (ii) Electrochemical response studies of the BSA/AAB-rGO/ITO immunoelectrode as a function of LDL concentrations (5−120 mg dL^{-1}), inset: a calibration curve has been plotted between R_{CT} values and the LDL concentration.

diffusion coefficients for NH_2-rGO/ITO, AAB-rGO/ITO, and BSA/AAB-rGO/ITO electrodes calculated using Randles-Sevcik equation are found to be as 6.6×10^{-6}, 77.24×10^{-6}, and 55.5×10^{-6} cm^2/s, respectively.

3.4. Impedance Spectroscopic Studies. Electrochemical impedance technique is an efficient, versatile tool for investigating the interfacial properties of layer formation due to biomolecules and electrode interaction. The transport of electrochemically produced charge can be modeled by capacitance/resistance changes occurring at the electrode/electrolyte interface of modified surfaces. The Randles equivalent circuit [inset, Figure 6(i)] includes the solution resistance (R_s), the Warburg impedance (Z_W) resulting from diffusion of the ions from the bulk electrolyte to the electrode interface, the double layer capacitance (C_{dl}), and electron transfer resistance (R_{CT}) due to redox species present in the electrolyte. The two components of the electronic circuit model namely, R_s and Z_W, represent bulk properties of the electrolyte solution and diffusion features of the redox probe in solution. Therefore, these parameters are not affected by chemical charge transfer occurring at the electrode surface. The other two components such as C_{dl} and R_{CT} depend on the dielectric and insulating features at the electrode/electrolyte interface. The Nyquist plot comprising of a semicircle diameter indicates the charge transfer resistance (R_{CT}) corresponding to the electron transfer limiting process at higher frequencies and a straight line intercept in the x-axis at 45° at the low frequencies revealing diffusion of the electrochemical species. Figure 6(i) shows the Nyquist plot of electrochemical impedance spectra (EIS) of (a) NH_2-rGO/ITO, (b) AAB-rGO/ITO, and (c) BSA/AAB-rGO/ITO electrodes in the PBS containing $K_3[Fe(CN)_6]/K_4[Fe(CN)_6]$, as a function of frequency ($0.01-10^4$ Hz) at fixed biasing potential 0.01 V. It is found that the R_{CT} value obtained for the NH_2-rGO/ITO electrode is 7.11 kΩ. After antibody immobilization, the R_{CT} value decreases to 2.01 kΩ indicating successful modification of the NH_2-rGO/ITO surface with antibodies. The decreased impedance may perhaps be due to orientation of antibodies with rGO sheets resulting in improved electron conduction toward the electrode. The values of impedance of the electrode before and after antibody immobilization are shown in Table II. The R_{CT} value increases by 3-fold (6.09 kΩ) after incorporation of the BSA molecules.

Table II. Equivalent Circuit Elements of Different Fabricated Electrodes

electrodes	R_s (Ω)	R_{CT} (kΩ)	C_{dl} (μF)	n
rGO/ITO	2.33×10^1	7.11	0.123	0.72
AAB- rGO/ITO	3.95×10^1	2.01	0.195	0.87
BSA/AAB-rGO/ITO	2.63×10^1	6.09	0.24	0.86

This can be attributed to the steric hindrance introduced by electrons during $K_3[Fe(CN)_6]/K_4[Fe(CN)_6]$ redox reaction. These electrodes have been characterized by analyzing the parameters such as HET (k_e) and time constant (τ). The corresponding k_e values of the modified electrodes can be calculated using eq 7[35]

$$k_e = \frac{RT}{n^2F^2AR_{CT}C} \tag{7}$$

where R is the gas constant, T is the temperature, n is the number of electrons transferring constant of the redox couple, F is Faraday constant, A is the effective area of the electrode, and C is the concentration of the redox couple in the bulk solution. The k_e value of the AAB-rGO/ITO electrode obtained as 1.33×10^{-4} cm/s is higher than that of the BSA/AAB-rGO/ITO bioelectrode (0.383×10^{-4} cm/s) indicating a faster electron exchange between the redox probes. The BSA-AAB immobilization on the NH_2-rGO/ITO electrode provides resistance to electron transfer resulting in decreased electron transfer rate constant and, consequently, generating low capacitance at the electrode surface. The observed high value of time constant (τ) for the BSA/AAB-rGO/ITO bioelectrode compared to that of the NH_2-rGO/ITO electrode is due to the slow diffusion of $[Fe(CN)_6]^{3-/4-}$ ions at the electrode enzyme layer/solution interface. The frequency associated with maximum $-Z''$ and R_{ct} has been calculated using the C_{dl} value via eq 8

$$R_{ct}C_{dl} = \frac{1}{2\pi f_{max}} = \tau \tag{8}$$

where f_{max} is the maximum frequency. The value of τ for NH_2-rGO/ITO is 0.874 ms, for AAB-rGO/ITO it is 0.392 ms, and for the BSA/AAB-rGO/ITO it is 1.462 ms.

dx.doi.org/10.1021/la4049852 | Langmuir 2014, 30, 4192−4201

Table III. Characteristics of the BSA-AAB/NH_2-rGO/ITO Immunosensor along with Those Reported in the Literature

detection method	detection range (mg/L)	sensitivity	detection limit (mg/L)	response time	stability	ref
SPR	100−1300	800 m° μm^{-1}	100	12,000 s	----	19
electrochemiluminescence	2.5×10^{-5}−0.016	----	6×10^{-6}	----	----	20
electrochemical	-----	-----	3.4×10^{-7}	3000 s	------	39
impedance	0.35−0.875	----	0.35	.....	----	36
impedance	50 − 1200	6120 Ω/(mg/L)/cm^2	0.5	250 s	5 weeks	present work

3.5. Impedimetric Detection. Electrochemical impedance studies of the BSA/AAB-rGO/ITO immunoelectrode have been conducted as a function of LDL concentration (5−120 mg dL^{-1}) [Figure 6(ii)]. The observed R_{CT} values of the BSA-AAB/RGO/ITO immunoelectrode obtained as a function of LDL concentration are shown in the inset of Figure 6(ii). The diameter of the Nyquist plot (R_{CT} value) increases with increasing LDL concentration, indicating that LDL molecules are absorbed onto the rGO electrode surface due to antigen−antibody interactions. The paratope of AAB (specific binding sites) allows these molecules to interact with epitope of LDL molecules. The higher concentration of LDL molecules may result in increased accumulation of immunocomplex at the sensor surface leading to enhanced impedance. A calibration curve has been obtained between the R_{CT} value and the LDL concentration (inset). It has been shown that the BSA/AAB-rGO/ITO immunoelectrode electrode has a detection range of 5−120 mg/dL. The normal range of LDL in a healthy human body is less than 100 mg/dL. This biosensor can be used to detect LDL concentration up to 120 mg/dL. After 120 mg/dL, the impedance response of this proposed biosensor is found to be saturated. This biosensor can detect a lower concentration of 5 mg dL^{-1} of LDL molecules. This may be assigned to the presence of oxygen-containing groups on the surface of the rGO which is responsible for strong capability of absorbing molecules along with enhanced surface concentration. The higher sensitivity obtained to be as 612 Ω mg^{-1} dL cm^{-2} for the BSA/AAB-rGO/ITO immunoelectrode indicates that the rGO based electrode is an interesting smart material for the fabrication of a biosensor. A typical plot between the logarithm of frequencies and impedance of the BSA/AAB-rGO/ITO immunoelectrode at 5 mg/dL of LDL concentration is shown in Figure S1. The impedance decreases with increase in frequency and becomes saturated at 10 Hz. Using the EIS method, the detection time for one LDL concentration is found to be 250 s (inset: Figure S1). Thus, this method provides lesser detection time compared to those with the other reported methods (Table III).[19,36] The rGO based impedimetric immunosensor provides a higher sensitivity in a wide detection range (5−120 mg/dL). The HET characteristics and functionality of rGO with biomolecules result in improved immunosensing characteristics. Table III shows the characteristics of this immunosensor along with those reported in the literature using other methods for LDL detection. It can be seen that the rGO integrated EIS method is an efficient, simple, low cost, and lesser time-consuming technique for LDL monitoring.

The kinetic analysis of the immunosensor has been investigated using EIS at room temperature (298 K). The binding reaction equation for the two macromolecular interactants is $[A] + [B] \Leftrightarrow [AB]$. The rate of formation of complex in the association phase is given as eq 9

$$\frac{d[AB]}{dt} = K_a[A][B] - k_d[AB] \quad (9)$$

where k_a and k_d are the association and dissociation rate constants. The observed values of association (k_d) and dissociation (k_d) rate constants for AAB-LDL binding are estimated to be as 1.66 M^{-1} s^{-1} and 0.6 s^{-1}, respectively. The equilibrium constant for association ($K_A = k_a/k_d$) is found to be as 2.77 M^{-1}. Zimple et al. have reported the values of association constant and dissociation constant of the AAB-LDL interaction in 4-aminothiophenol as 96.7 M^{-1} s^{-1} and 0.000264 × s^{-1} using SPR.[37] Ali et al. have observed that the values of k_a and k_d are 33.4 k M^{-1} s^{-1} and 0.0896 s^{-1}, respectively.[38] The equilibrium constant of this biosensor is found to be lower compared to those reported in literature.[37,38] The observed dissociation constant (k_d) of this proposed biosensor has been found to be higher (0.6 s^{-1}) compared to the reported value[37] resulting in a low equilibrium constant. However, the k_a value is observed to be lower 1.66 M^{-1} s^{-1} due to the presence of rGO interaction with AAB molecules on the transducer surface. Thus, the higher K_a of the BSA/AAB-rGO/ITO immunoelectrode reveals strong binding affinity with LDL molecules. The reproducibility of the different BSA/AAB-rGO/ITO immunoelectrodes has been investigated at LDL concentration of 60 mg/dL, and no significant change in the R_{CT} value for four electrodes is found as evidenced by the low relative standard deviation (RSD) of 1.48% (n = 4), indicating good precision [inset: Figure S2]. The BSA/AAB-rGO/ITO immunoelectrode shows good repeatability as evidenced by the RSD 4.4% (n = 13) for LDL (60 mg/dL) concentration, after 13 times washing/repetition of the immunoelectrode [Figure S2]. No significant decrease in charge transfer resistance is observed after using it 12 times after which the immunoelectrode shows a significant decrease (∼30%) in impedance. This is perhaps due to denaturation of the antibodies. The shelf life of the BSA/AAB-rGO/ITO immunoelectrode measured after an interval of 1 week has been estimated to be as 7 weeks when the immunoelectrode is stored at 4 °C when not in use.

4. CONCLUSIONS

We have demonstrated the fabrication of a label free immunosensor using antibody functionalized aminated rGO for detection of lipid molecules via impedance spectroscopy. The NH_2 groups have been introduced on the edges of the rGO sheet by replacement of COCl groups to amide groups (CO-NH). The synthesized NH_2-rGO plays an important role for lipid functionalization via covalent interaction of -NH_2 and -COOH groups. The change in impedance signal of the fabricated immunosensor due to immunocomplex formation on the surface has been investigated. The observed higher sensitivity (612 Ω/mg dL^{-1} cm^{-2}) and long-term stability of 5 weeks suggest potential application of this immunoelectrode in clinical diagnostics. This BSA/AAB-rGO/ITO immunosensor exhibits linearity in the range of 15−90 mg/dL with fast

dx.doi.org/10.1021/la4049852 | Langmuir 2014, 30, 4192−4201

detection time (250 s), high stability, and reproducibility. This rGO-based EIS strategy can perhaps be used for the development of bioanalytical devices for POC diagnostic tests. Efforts are being made to utilize this rGO-based interface for investigation of other lipid−lipid interactions and detection of clinically important biomolecules including triglycerides and esterified cholesterol.

■ ASSOCIATED CONTENT

Supporting Information

Figures S1 and S2. This material is available free of charge via the Internet at http://pubs.acs.org.

■ AUTHOR INFORMATION

Corresponding Authors

*Phone: +91-011-27294668. Fax: +91-011-27871023. E-mail: bansi.malhotra@dce.ac.in.
*E-mail: ved.varun@gmail.com.
*E-mail: renujohn@iith.ac.in.

Author Contributions

[$]These authors have equally contributed.

Notes

The authors declare no competing financial interest.

■ ACKNOWLEDGMENTS

We thank the Director, CSIR-National Physical Laboratory, New Delhi, India for providing the facilities. Md. A. Ali and S.S. acknowledge CSIR, New Delhi, India for the financial support. We thank Dr. Vinod Kumar and Dr. Anchal Srivastava (BHU, India) for interesting discussions relating to synthesis of rGO. V.V.A. is thankful to TSDP-DST and CSIR empower project for funding. We thank K. N. Sood, NPL, New Delhi for elemental analysis. The financial support received from the Department of Science and Technology, India (Grant No. DST/TSG/ME/2008/18) and the Indian Council of Medical Research, India (Grant No. ICMR/5/3/8/91/GM/2010-RHN) is gratefully acknowledged.

■ REFERENCES

(1) Ohno, Y.; Maehashi, K.; Matsumoto, K. Label-Free Biosensors Based on Aptamer-Modified Graphene Field-Effect Transistors. *J. Am. Chem. Soc.* **2010**, *132*, 18012−18013.

(2) Song, Y.; Zhang, Y.; Bernard, P. E.; Reuben, J. M.; Ueno, N. T.; Arlinghaus, R. B.; Zu, Y.; Qin, L. Multiplexed Volumetric Bar-Chart Chip for Point-of-Care Diagnostics. *Nat. Commun.* **2012**, *3*, 1283.

(3) Cho, H.; Yeh, E.-C.; Sinha, R.; Laurence, T. A.; Bearinger, J. P.; Lee, L. P. Single-Step Nanoplasmonic $VEGF_{165}$ Aptasensor for Early Cancer Diagnosis. *ACS Nano* **2012**, *6*, 7607−7614.

(4) Ali, M. A.; Solanki, P. R.; Patel, M. K.; Dhayani, H.; Agrawal, V. V.; John, R.; Malhotra, B. D. A Highly Efficient Microfluidic Nano Biochip Based on Nanostructured Nickel Oxide. *Nanoscale* **2013**, *5*, 2883.

(5) Kamil Reza, K.; Singh, M. K.; Yadav, S. K.; Singh, J.; Agrawal, V. V.; Malhotra, B. D. Quantum Dots Based Platform for Application to Fish Freshness Biosensor. *Sens. Actuators, B* **2013**, *177*, 627−633.

(6) Ali, M. A.; Srivastava, S.; Solanki, P. R.; Reddy, V.; Agrawal, V. V.; Kim, C.; John, R.; Malhotra, B. D. Highly Efficient Bienzyme Functionalized Nanocomposite-Based Microfluidics Biosensor Platform for Biomedical Application. *Sci. Rep.* **2013**, *3*.

(7) Geim, A. K. Graphene: Status and Prospects. *Science* **2009**, *324*, 1530−1534.

(8) Geim, A. K.; Novoselov, K. S. The Rise of Graphene. *Nat. Mater.* **2007**, *6*, 183−191.

(9) Pumera, M.; Ambrosi, A.; Bonanni, A.; Chng, E. L. K.; Poh, H. L. Graphene for Electrochemical Sensing and Biosensing. *TrAC, Trends Anal. Chem.* **2010**, *29*, 954−965.

(10) Robinson, J. T.; Perkins, F. K.; Snow, E. S.; Wei, Z.; Sheehan, P. E. Reduced Graphene Oxide Molecular Sensors. *Nano Lett.* **2008**, *8*, 3137−3140.

(11) Stankovich, S.; Dikin, D. A.; Dommett, G. H. B.; Kohlhaas, K. M.; Zimney, E. J.; Stach, E. A.; Piner, R. D.; Nguyen, S. T.; Ruoff, R. S. Graphene-Based Composite Materials. *Nature* **2006**, *442*, 282−286.

(12) Shao, Y.; Wang, J.; Wu, H.; Liu, J.; Aksay, I. A.; Lin, Y. Graphene Based Electrochemical Sensors and Biosensors: A Review. *Electroanalysis* **2010**, *22*, 1027−1036.

(13) Yang, Y.; Asiri, A. M.; Tang, Z.; Du, D.; Lin, Y. Graphene Based Materials for Biomedical Applications. *Mater. Today* **2013**, *16*, 365−373.

(14) Pumera, M. Graphene-Based Nanomaterials and Their Electrochemistry. *Chem. Soc. Rev.* **2010**, *39*, 4146.

(15) Becerril, H. A.; Mao, J.; Liu, Z.; Stoltenberg, R. M.; Bao, Z.; Chen, Y. Evaluation of Solution-Processed Reduced Graphene Oxide Films as Transparent Conductors. *ACS Nano* **2008**, *2*, 463−470.

(16) Zhou, M.; Zhai, Y.; Dong, S. Electrochemical Sensing and Biosensing Platform Based on Chemically Reduced Graphene Oxide. *Anal. Chem.* **2009**, *81*, 5603−5613.

(17) Compton, O. C.; Jain, B.; Dikin, D. A.; Abouimrane, A.; Amine, K.; Nguyen, S. T. Chemically Active Reduced Graphene Oxide with Tunable C/O Ratios. *ACS Nano* **2011**, *5*, 4380−4391.

(18) Li, J.; Lu, C.-H.; Yao, Q.-H.; Zhang, X.-L.; Liu, J.-J.; Yang, H.-H.; Chen, G.-N. A Graphene Oxide Platform for Energy Transfer-Based Detection of Protease Activity. *Biosens. Bioelectron.* **2011**, *26*, 3894−3899.

(19) Liu, Y.; Yu, D.; Zeng, C.; Miao, Z.; Dai, L. Biocompatible Graphene Oxide-Based Glucose Biosensors. *Langmuir* **2010**, *26*, 6158−6160.

(20) Eda, G.; Fanchini, G.; Chhowalla, M. Large-Area Ultrathin Films of Reduced Graphene Oxide as a Transparent and Flexible Electronic Material. *Nat. Nanotechnol.* **2008**, *3*, 270−274.

(21) Lai, L.; Chen, L.; Zhan, D.; Sun, L.; Liu, J.; Lim, S. H.; Poh, C. K.; Shen, Z.; Lin, J. One-Step Synthesis of NH_2-Graphene from in Situ Graphene-Oxide Reduction and Its Improved Electrochemical Properties. *Carbon* **2011**, *49*, 3250−3257.

(22) Srivastava, S.; Kumar, V.; Ali, M. A.; Solanki, P. R.; Srivastava, A.; Sumana, G.; Saxena, P. S.; Joshi, A. G.; Malhotra, B. D. Electrophoretically Deposited Reduced Graphene Oxide Platform for Food Toxin Detection. *Nanoscale* **2013**, *5*, 3043.

(23) Wan, Y.; Lin, Z.; Zhang, D.; Wang, Y.; Hou, B. Impedimetric Immunosensor Doped with Reduced Graphene Sheets Fabricated by Controllable Electrodeposition for the Non-Labelled Detection of Bacteria. *Biosens. Bioelectron.* **2011**, *26*, 1959−1964.

(24) Lisdat, F.; Schäfer, D. The Use of Electrochemical Impedance Spectroscopy for Biosensing. *Anal. Bioanal. Chem.* **2008**, *391*, 1555−1567.

(25) Siddiqui, S.; Arumugam, P. U.; Chen, H.; Li, J.; Meyyappan, M. Characterization of Carbon Nanofiber Electrode Arrays Using Electrochemical Impedance Spectroscopy: Effect of Scaling Down Electrode Size. *ACS Nano* **2010**, *4*, 955−961.

(26) Nauck, M.; Warnick, G. R.; Rifai, N. Methods for Measurement of LDL-Cholesterol: A Critical Assessment of Direct Measurement by Homogeneous Assays versus Calculation. *Clin. Chem.* **2002**, *48*, 236−254.

(27) Matharu, Z.; Arya, S. K.; Sumana, G.; Gupta, V.; Malhotra, B. D. Self-Assembled Monolayer for Low Density Lipoprotein Detection. *J. Mol. Recognit.* **2008**, *21*, 419−424.

(28) Jie, G.; Liu, B.; Pan, H.; Zhu, J.-J.; Chen, H.-Y. CdS Nanocrystal-Based Electrochemiluminescence Biosensor for the Detection of Low-Density Lipoprotein by Increasing Sensitivity with Gold Nanoparticle Amplification. *Anal. Chem.* **2007**, *79*, 5574−5581.

(29) Awasthi, K.; Singh, D. P.; Singh, S. K.; Dash, D.; Srivastava, O. N. Attachment of Biomolecules (Protein and DNA) to Amino-

Functionalized Carbon Nanotubes. *New Carbon Mater.* **2009**, *24*, 301−306.
(30) Sarkar, P.; Nicholson, P. S. Electrophoretic Deposition (EPD): Mechanisms, Kinetics, and Application to Ceramics. *J. Am. Ceram. Soc.* **1996**, *79*, 1987−2002.
(31) Srivastava, S.; Solanki, P. R.; Kaushik, A.; Ali, M. A.; Srivastava, A.; Malhotra, B. D. A Self Assembled Monolayer Based Microfluidic Sensor for Urea Detection. *Nanoscale* **2011**, *3*, 2971.
(32) Liu, Y.-H.; Li, H.-N.; Chen, W.; Liu, A.-L.; Lin, X.-H.; Chen, Y.-Z. Bovine Serum Albumin-Based Probe Carrier Platform for Electrochemical DNA Biosensing. *Anal. Chem.* **2013**, *85*, 273−277.
(33) Watt-Smith, M. J.; Friedrich, J. M.; Rigby, S. P.; Ralph, T. R.; Walsh, F. C. Determination of the Electrochemically Active Surface Area of Pt/C PEM Fuel Cell Electrodes Using Different Adsorbates. *J. Phys. Appl. Phys.* **2008**, *41*, 174004.
(34) Wright, J. E. I.; Cosman, N. P.; Fatih, K.; Omanovic, S.; Roscoe, S. G. Electrochemical Impedance Spectroscopy and Quartz Crystal Nanobalance (EQCN) Studies of Insulin Adsorption on Pt. *J. Electroanal. Chem.* **2004**, *564*, 185−197.
(35) Kaushik, A.; Solanki, P. R.; Kaneto, K.; Kim, C. G.; Ahmad, S.; Malhotra, B. D. Nanostructured Iron Oxide Platform for Impedimetric Cholesterol Detection. *Electroanalysis* **2010**, *22*, 1045−1055.
(36) Oliveira, M. D. L.; Abdalla, D. S. P.; Guilherme, D. F.; Faulin, T. E. S.; Andrade, C. A. S. Impedimetric Immunosensor for Electronegative Low Density Lipoprotein (LDL−) Based on Monoclonal Antibody Adsorbed on (polyvinyl Formal)−gold Nanoparticles Matrix. *Sens. Actuators, B* **2011**, *155*, 775−781.
(37) Matharu, Z.; Bandodkar, A. J.; Sumana, G.; Solanki, P. R.; Ekanayake, E. M. I. M.; Kaneto, K.; Gupta, V.; Malhotra, B. D. Low Density Lipoprotein Detection Based on Antibody Immobilized Self-Assembled Monolayer: Investigations of Kinetic and Thermodynamic Properties. *J. Phys. Chem. B* **2009**, *113*, 14405−14412.
(38) Ali, M. A.; Srivastava, S.; Pandey, M. K.; Agrawal, V. V.; John, R.; Malhotra, B. D. Protein−Conjugated Quantum Dots Interface: Binding Kinetics and Label-Free Lipid Detection. *Anal. Chem.* **2014**, *86*, 1710−1718.
(39) Yan, W.; Chen, X.; Li, X.; Feng, X.; Zhu, J.-J. Fabrication of a Label-Free Electrochemical Immunosensor of Low-Density Lipoprotein. *J. Phys. Chem. B* **2008**, *112*, 1275−1281.